PROCEEDINGS OF SCIENCE

Reactions of neutron-rich Sn isotopes investigated at relativistic energies at R^{3}B

Fabia Schindler[*†]
for the R^{3}B collaboration
Technische Universität Darmstadt
E-mail: fa.schindler@gsi.de

Reactions of neutron-rich Sn isotopes have been measured in inverse kinematics at the R^{3}B-setup at GSI in Darmstadt in 2012. Due to the neutron excess, which results in a weaker binding of the valence neutrons such isotopes are expected to form a very neutron-rich surface, the neutron skin. The investigation of this phenomenon is one of the main goals of the experiment. The reaction products of the isotopes ^{124}Sn to ^{134}Sn have been measured at beam energies of 300 *A*MeV to 600 *A*MeV in a kinematically complete way. Different reaction channels will be analyzed, therefore information about the neutron skin can be obtained from different methods. These are in particular the neutron removal cross sections and the dipole polarizability of the nucleus, which are both sensitive to the neutron-skin thickness. The latter will be obtained from the differential cross section of electromagnetic excitation measured in a wide excitation-energy range including the Pygmy and Giant Dipole Resonances. Furthermore, the mass dependency of the neutron skin within the measured isotopic chain will be analyzed.

52 International Winter Meeting on Nuclear Physics - Bormio 2014,
27-31 January 2014
Bormio, Italy

[*]Speaker.

[†]This work is supported by the BMBF project 05P12RDFN8, the GSI TU-Darmstadt Cooperation, HIC for FAIR and NAVI.

PoS(Bormio2014)009

1. Introduction

The atomic nucleus is a complex many-body system bound by the strong force. One of the main challenges in nuclear physics is the investigation of the properties of nuclei, which can show a variety of structures, depending on the proton to neutron ratio.
The properties of stable nuclei are relatively well known and can be described in theoretical frameworks like the shell model [1, 2] over a wide mass range. Away from the valley of stability the situation changes drastically. Conventional models lose their validity and nuclei can form exotic structures.
Exotic nuclei usually have a large proton to neutron asymmetry compared to stable nuclides. Isotopes with the maximum number of bound neutrons (protons) build the neutron (proton) drip line of the nuclear landscape. Single nucleons which are less bound to the nucleus are called halos. A prominent example is the nucleus ^{11}Li, which consists of a ^{9}Li core and two additional neutrons forming the halo [3]. On the way to higher neutron numbers an other phenomenon is of great interest for nuclear-structure physics. Due to the different Fermi levels of protons and neutrons the matter radii of the different nucleon species in the nucleus differ. This phenomenon can lead to a neutron-rich surface of the nucleus, the neutron skin.
Besides improving the knowledge about nuclear structure in general the investigation of exotic nuclei is also of great interest in the field of astrophysics. Exotic nuclei play for instance an important role for the synthesis of heavy elements in the universe. Furthermore, experiments with neutron-rich isotopes are a possibility to probe a kind of matter which is expected to appear in compact objects like neutron stars.
Reactions induced by heavy-ion collisions have been proven to be an excellent tool for the investigation of nuclear structure. The measurement of the properties of the reaction products allows to draw conclusions about the structure of the projectile nucleus. Due to the great development in the field of accelerator physics, the production of heavy unstable isotopes with relativistic energies has become possible. For that reason properties of exotic nuclei can be studied by this kind of experiments.
The investigation of the reactions and therefore the structure of neutron-rich Sn isotopes in the mass region from $A = 124$ to $A = 134$ was the purpose of the experiment S412 presented here, which was performed at the R^{3}B-setup at GSI in Darmstadt in spring 2012. The experimental setup is introduced in section 2. Since tin is charged by 50 protons, the measured isotopes have a considerable neutron excess and are expected to form a neutron skin. The investigation of this phenomenon, in particular the determination of the neutron-skin thickness from experimental data, allows to place important constraints on the equation of state (EOS) of asymmetric nuclear matter as described in section 3. Two independent reaction channels will be analyzed to extract the neutron-skin thickness. These are nuclear reactions caused by the collisions of the projectiles with a $^{\text{nat}}$C target on the one hand and Coulomb excitations induced by a $^{\text{nat}}$Pb target on the other hand. The analysis of the different reaction mechanisms requires different techniques as described in section 4.

2. The R^{3}B-setup

The experimental setup for studies of Reactions with Relativistic Radioactive Beams (R^{3}B) is located at GSI. The primary beam of stable nuclei accelerated in the synchrotron SIS18 is used to produce a secondary beam of radioactive isotopes by reactions with a production target located in front of the FRagment Separator FRS. For the S412 experiment, a primary beam of ^{136}Xe was used to produce the nuclei of interest in the lower mass region (^{124}Sn-^{129}Sn) via fragmentation. The heavier isotopes (^{130}Sn-^{134}Sn) are fission products from the reaction of ^{238}U with the production target. To separate the Sn isotopes from the variety of produced particles, as described in the text below, the magnetic rigidity $B\rho$ of the isotopes has to be obtained. The secondary beam enters the experimental hall shown in Figure 1 with relativistic energies of 300 *A*MeV to 600 *A*MeV.

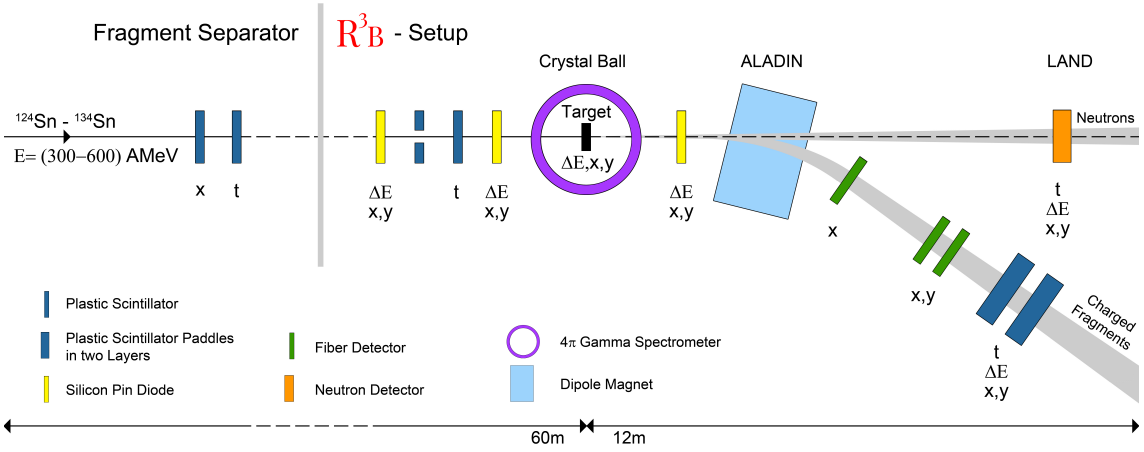

Figure 1: The R^{3}B-setup at GSI as described in the text.

The R^{3}B-setup allows for a kinematically complete measurement of reactions, which means that all of the reaction products including charged fragments, neutrons and gamma rays are detected. Different detectors are located in front of the target to identify the incoming isotopes. The measured observables are the position x, y and the arrival time t at a certain detector as well as the energy loss ΔE in the detector material, as labeled in Figure 1. The velocity β of the isotopes is calculated from the time of flight measurement between two plastic scintillators with a distance of about 55 m and used to determine the charge Z of the isotopes from the energy loss $\Delta E \propto Z^2/\beta^2$ in a silicon pin diode.

The massnumber A of the incoming isotopes can be reconstructed from position measurements at the FRS. The trajectory of an ion with charge q and relativistic momentum p traveling through a magnetic field is given by a circular path with radius ρ. Since the field strength B of the FRS magnets is known and the projectiles are fully stripped ($q = Ze$) the mass number A of the isotopes can be obtained from relation $B\rho = \frac{p}{q} \propto \frac{A}{Z}\beta\gamma$ with $\gamma = 1/\sqrt{1-\beta^2}$. Figure 2 shows an example for an incoming particle identification plot, which covers the heavy mass region.

Behind the target the charged reaction products are deflected due to the magnetic field of the dipole magnet ALADIN. The detectors located along the fragment path allow for a charge and mass identification based on the same techniques as used for the incoming isotopes.

The neutrons pass the magnetic field on a straight line and are detected by the Large Area Neutron Detector (LAND). The measurement of gamma rays is realized by the 4π gamma spectrometer Crystal Ball consisting of 162 NaI crystals surrounding the target.

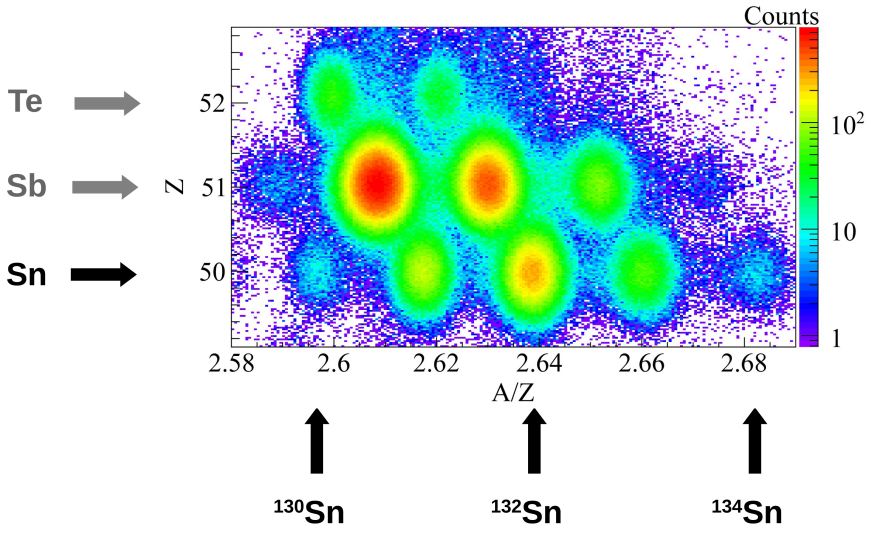

Figure 2: Example for an incoming particle identification plot covering the heavy mass region. Shown is the charge Z of the isotopes vs the mass to charge ratio A/Z.

3. The EOS of asymmetric nuclear matter

Due to the versatility of experimental methods which can be used for the study of stable nuclei, the EOS of symmetric nuclear matter is well investigated. The number of open questions is increasing by adding additional neutrons to the nucleus and a detailed description of neutron-rich matter still has to be found. A common parameterization for the EOS of asymmetric nuclear matter is given in [4]

$$e(\rho,\delta) = e(\rho,0) + S(\rho)\,\delta^2 + \mathscr{O}\left(\delta^4\right). \tag{3.1}$$

The asymmetry parameter $\delta = (\rho_n - \rho_p)/\rho$ is the quantity describing the neutron excess depending on the neutron and proton density distributions ρ_n and ρ_p with $\rho = \rho_n + \rho_p$. The first part of equation (3.1) is the EOS of symmetric nuclear matter $e(\rho,0)$. The deviation of the EOS from the symmetric part is highly dependent on the parameter

$$S(\rho) = \frac{1}{2}\frac{\partial e(\rho,\delta)}{\partial \delta^2}|_{\delta=0} \tag{3.2}$$

called the symmetry energy.

To achieve a precise description of asymmetric nuclear matter the task is to place constraints on the parameters of the EOS. For this reason correlations between quantities describing the EOS and observables which can be extracted from experimental data have to be found. An example for this is given in [5]. Figure 3 shows the linear correlation between the neutron skin thickness ΔR, which is defined as the difference of the neutron and proton root-mean-square radii

$$\Delta R = \langle r^2 \rangle_n^{\frac{1}{2}} - \langle r^2 \rangle_p^{\frac{1}{2}} \tag{3.3}$$

and the derivative of the EOS of neutron matter at a density close to saturation. The data shown in Figure 3 is based on Hartree-Fock calculations with different Skyrme parameter sets (circles) and has been adopted from [5]. In addition different relativistic models (squares) were used.

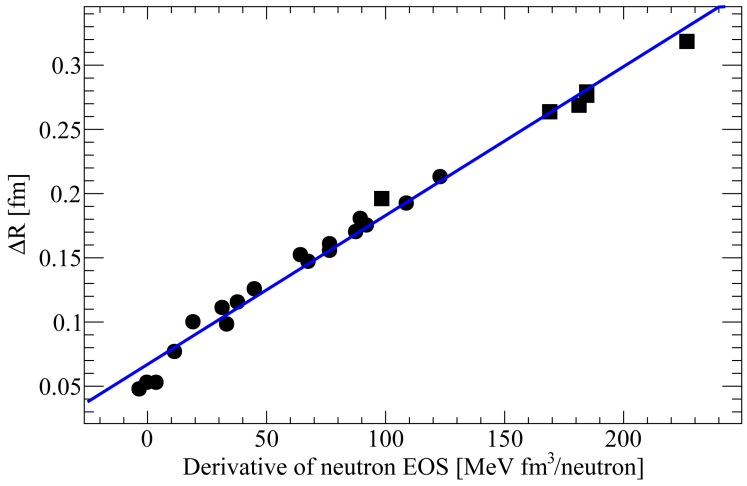

Figure 3: The neutron-skin thickness ΔR in ^{208}Pb vs the derivative of the neutron EOS. The calculations are based on Hartree-Fock using different Skyrme parameter sets (circles) and relativistic models (squares). The data is adopted from [5].

4. The neutron-skin thickness

One of the main goals of experiment S412 was the investigation of the neutron-skin thickness in the measured Sn isotopes which can be extracted from two independent methods, nuclear reactions as well as Coulomb excitations. The underlying analysis techniques are presented in this section.

4.1 Nuclear reactions

To analyse nuclear reactions of the projectile a target with low charge number has to be chosen. For this purpose measurements with a ^{nat}C target have been performed in the experiment. Figure 4 shows a simplified geometrical model of the collision with an impact parameter b which is defined as the distance between the projectile and the target nucleus. For small values of b the collision results in fragmentation or the knockout of nucleons from both species. By increasing the impact parameter to a value where the overlap between target and projectile nucleus only affects the projectiles neutron skin, which is schematically drawn in blue, the knockout of protons is expected to be very unlikely. In that case the projectile protons do not scatter and one ore more neutrons are removed. Therefore, the total reaction cross section σ_{tot} can be separated into two parts

$$\sigma_{tot} = \sigma_{\Delta Z} + \sigma_{\Delta N}. \tag{4.1}$$

$\sigma_{\Delta Z}$ includes all the reactions leading to the loss of at least one proton. The total neutron removal cross section $\sigma_{\Delta N}$ covers the reactions for which only neutrons are removed and is sensitive to the neutron-skin thickness.

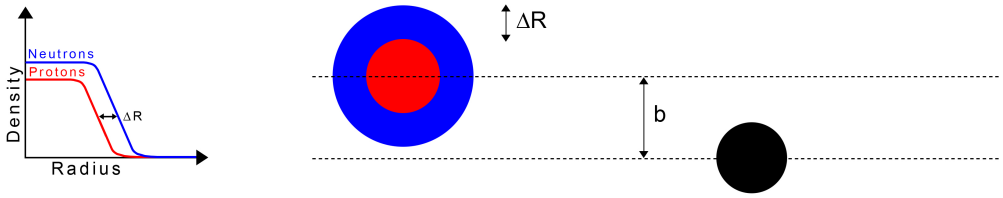

Figure 4: Schematic picture of the collision between a neutron-rich projectile and a ^{nat}C target nucleus with impact parameter b. The projectiles neutron-skin thickness ΔR is defined as the difference of the neutron and proton root-mean-square radii.

A theoretical description of $\sigma_{\Delta N}$ can be derived from the probability approach in eikonal approximation [6]. The cross section of the removal of N_X neutrons out of a (N_{Proj},Z_{Proj}) projectile can be expressed as

$$\sigma_{N_X} = \begin{pmatrix} N_{Proj} \\ N_X \end{pmatrix} \int d^2b \left[1 - P_n(b)\right]^{N_X} \left[P_n(b)\right]^{N_{Proj}-N_X} \left[P_p(b)\right]^{Z_{Proj}}. \tag{4.2}$$

The first part of equation (4.2) is the number of possibilities for selecting N_X neutrons out of the projectile neutrons N_{Proj}. The integral over the impact parameter includes the probability distributions $P(b)$ for the persistence of each projectile nucleon in the core. These probability distributions are dependent on the free nucleon-nucleon cross sections σ_{np} and σ_{pp} and the nucleon density distributions ρ_n and ρ_p which have to be taken from a theoretical model. If the model is chosen in a way that the theoretical cross section

$$\sigma_{\Delta N} = \sum \sigma_{N_X} \tag{4.3}$$

agrees with the measured one, the neutron-skin thickness can be obtained from the nucleon density distributions.

4.2 Coulomb excitations

To achieve electromagnetic excitation of the projectiles, a ^{nat}Pb target was used in the experiment. In order to subtract the background radiation and effects from nuclear reactions which contaminate the data, measurements with a ^{nat}C target and an empty target frame were performed as well.

The Coulomb breakup reaction cross section can be described in the equivalent photon method. The reaction process is illustrated in Figure 5 and a detailed description can be found in [7]. The excitation is treated like an exchange of a virtual photon between target and projectile nucleus and results in the removal of a neutron. In case of an electric-dipole excitation (E1) the cross section can be written [8]

$$\frac{d\sigma(E)}{dE} = \frac{16\pi^3}{9\hbar c} N_{\mathrm{E1}}(E) \frac{dB(\mathrm{E1})}{dE}, \tag{4.4}$$

where N_{E1} is the number of virtual photons and $B(\mathrm{E1})$ is the transition probability.

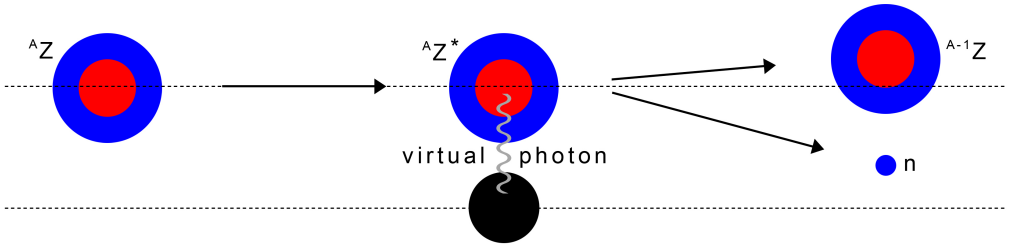

Figure 5: Schematic picture of the Coulomb excitation in a neutron-rich projectile caused by a $^{\mathrm{nat}}$Pb target. The excitation can be described as an exchange of a virtual photon between the projectile and target nucleus and results e.g. in the removal of a neutron.

Since the R^{3}B-setup allows for kinematically complete measurements, the four-momenta of all reaction products are known and the excitation energy E can be deduced from the invariant-mass technique

$$E = \sqrt{\sum_i m_i^2 + \sum_{i \neq j} \gamma_i \gamma_j m_i m_j \left(1 - \beta_i \beta_j \cos \vartheta_{ij}\right)} + E_\gamma - m_{Proj}, \tag{4.5}$$

where the indices i and j run over all reaction products, with the four-momenta forming an angle ϑ_{ij}. E_γ is the energy of the measured photons.
From the Coulomb breakup cross section (4.4) the dipole polarizability α_D can be directly obtained. α_D is defined as

$$\alpha_D = \frac{8\pi}{9} \int_0^\infty \frac{dB(E1)}{E} \tag{4.6}$$

and was found to be highly sensitive to the neutron-skin thickness (see text below).
Recently the results of the α_D measurement in ^{68}Ni were published in [9]. The corresponding experiment was also performed at the R^{3}B-setup and provided the first measurement of α_D in an unstable neutron-rich nucleus. The experimental E1 strength distribution obtained in this work is shown in Figure 6. Contributions from the Giant as well as from the Pygmy Dipole Resonances can be clearly identified. The dipole polarizability is determined from equation (4.6) and amounts to α_D=3.40(23) fm^3. A linear correlation between α_D and the neutron-skin thickness is shown in Figure 7. The calculations from [10] are based on a mean-field model with FSUGold interaction and were used in [9] to deduce the neutron-skin thickness in ^{68}Ni, which is found to be ΔR=0.17(2) fm.

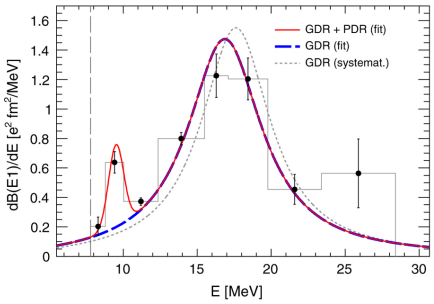

Figure 6: Experimental E1 strength distribution (histogram and data points) of ^{68}Ni obtained in [9]. The fit function describing the Giant and Pygmy Dipole Resonance contributions is shown in red. The one-neutron separation threshold is marked at 7.792 MeV. The figure is taken from [9].

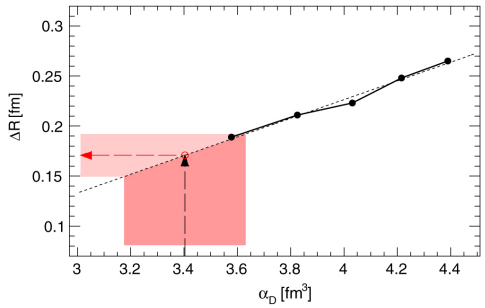

Figure 7: Correlation between the neutron skin thickness and the dipole polarizability in ^{68}Ni [9]. The experimental result for α_D from [9] is compared to mean-field calculations from [10] based on FSUGold interactions with different parameterizations of the symmetry energy. The figure is taken from [9].

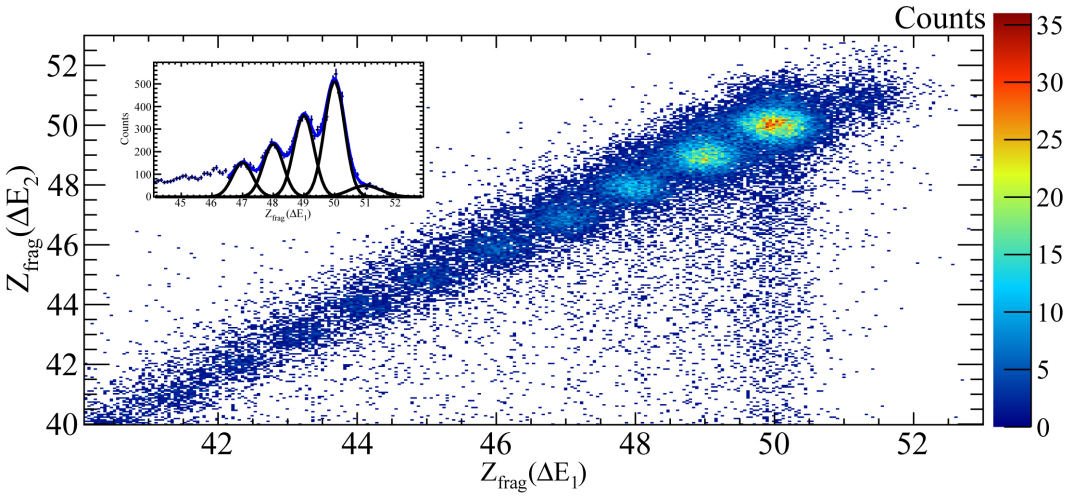

Figure 8: Fragment charges from nuclear reactions of ^{124}Sn with a ^{nat}C target. The two dimensional plot shows the correlation of the fragment charges obtained from the measured energy loss in a silicon pin diode (ΔE_1) directly behind the target and a time of flight wall (ΔE_2) located at the very end of the fragment path. The best charge resolution $\tilde{\sigma}_Z/Z \approx 0.7\%$ is achieved by a silicon pin diode (inset).

5. Preliminary results and outlook

Reactions of neutron-rich Sn isotopes have been measured at the R^{3}B-setup at GSI to investigate properties like the neutron-skin thickness and their behavior along the isotopic chain.
The resolution of the measured fragment charge is $\tilde{\sigma}_Z/Z \approx 0.7\%$, which leads to an adequate separation of the different outgoing isotopes as shown in Figure 8. The fragment-mass identification is currently ongoing and the last required calibration step to extract the neutron-skin thickness of the

isotopes from the analysis of nuclear reactions as described in section (4.1).
Furthermore, the Coulomb excitation of the projectiles will be analyzed over a wide excitation-energy range including the Giant as well as the Pygmy Dipole Resonances. The neutron-skin thickness will be extracted from the measured dipole polarizability as discussed in section (4.2).
In summary, the data of the S412 experiment will enable the investigation and comparison of the neutron-skin thickness extracted from two independent methods in the neutron-rich Sn isotopes from ^{124}Sn to ^{134}Sn.

References

[1] M. G. Mayer, *On Closed Shells in Nuclei. II*, *Physical Review* **75**, 1969, (1949)

[2] M. Haxel *et al.*, *On the "Magic Numbers" in Nuclear Structure*, *Physical Review* **75**, 1766, (1949)

[3] I. Tanihata *et al.*, *Measurements of interaction cross sections and nuclear radii in the light p-shell region*, *Physical Review Letters* **55**, 2676, (1985)

[4] X. Viñas *et al.*, *Density dependence of the symmetry energy from neutron skin thickness in finite nuclei*, *European Physical Journal A* **50**, 27, (2014)

[5] S. Typel *et al.*, *Neutron radii and the neutron equation of state in relativistic models*, *Physical Review C* **64**, 027302, (2001)

[6] C. A. Bertulani, *private communication*

[7] T. Aumann *et al.*, *The electric dipole response of exotic nuclei*, *Physica Scripta Volume T* **152**, 014012, (2013)

[8] C. A. Bertulani *et al.*, *Electromagnetic processes in relativistic heavy ion collisions*, *Physics Reports* **163**, 299, (1988)

[9] D. M. Rossi *et al.*, *Measurement of the Dipole Polarizability of the Unstable Neutron-Rich Nucleus* ^{68}*Ni*, *Physical Review Letters* **111**, 242503, (2013)

[10] J. Piekarewicz, *Pygmy resonances and neutron skin*, *Physical Review C* **83**, 034319, (2011)